Journal of Crystal Growth 405 (2014) 81–86

Contents lists available at ScienceDirect

Journal of Crystal Growth

journal homepage: www.elsevier.com/locate/jcrysgro

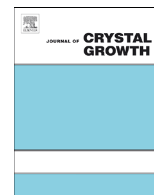

Defect reduction in epitaxial InP on nanostructured Si (001) substrates with position-controlled seed arrays

Qiang Li [a], Kar Wei Ng [a], Chak Wah Tang [a], Kei May Lau [a,*], Richard Hill [b], Alexey Vert [b]

[a] Department of Electronic and Computer Engineering, Hong Kong University of Science and Technology, Clear Water Bay, Kowloon, Hong Kong
[b] SEMATECH, 257 Fuller Road, Suite 2200, Albany, NY 12203, USA

ARTICLE INFO

Article history:
Received 10 April 2014
Received in revised form
4 July 2014
Accepted 29 July 2014
Communicated by: R. M. Biefeld
Available online 5 August 2014

Keywords:
A1. Defects
A3. Metal–organic chemical vapor deposition
B1. Nanomaterials
B2. Semiconducting III–V materials
B2. Semiconducting indium phosphide

ABSTRACT

Defect reduction in epitaxial InP on nanopatterned exact Si (001) substrates was investigated. Top-down lithography and dry etching were used to define 30 nm-wide SiO_2 trench openings, with concaves recessed into the Si substrates. Uniformly distributed and position-controlled InP seed arrays were formed by selective area growth. Afterwards, the SiO_2 mask was removed and InP overgrowth on the seed arrays proceeded. By localizing defects in the buried Si concaves and promoting defect interactions during the coalescence process, a significant reduction in the x-ray linewidth has been achieved for InP layers grown on the nanopatterned Si as compared to blanket epitaxy. Anisotropic defect distribution in the coalesced InP films was observed and its dependency on seed layer thickness was also studied.
© 2014 Elsevier B.V. All rights reserved.

1. Introduction

InP is one of the most essential photonic and electronic materials. Over the last few decades, InP and associated heterostructures have enabled long wavelength lasers [1], photodetectors [2], high-frequency and high-speed devices such as heterojunction bipolar transistors [3], high-electron mobility transistors [4] and metal-oxide-semiconductor field effect transistors [5]. To obtain the best device performance, most of these state-of-the-art devices are grown and fabricated on lattice-matched, but relatively costly and fragile InP substrates. Tremendous benefits could be attained by growing high crystalline quality InP on Si substrates, which are available with large diameter (up to 300 mm), lower cost, good thermal conductivity and mechanical property. More significantly, such heteroepitaxy technique can take full advantage of the well-established Si manufacturing base, and open the venue for monolithic integration of a wide range of photonic and electronic components on a common platform [6,7].

However, heteroepitaxy of InP and related alloys on Si is challenging due to the 8% lattice mismatch, large thermal mismatch and the polar/non-polar nature of the III–V/IV system. Conventional growth on planar Si wafers usually involves thick transitional buffers such as GaP [8], GaAs [9–11], InAlAs/GaAs/Ge [12] or InAlAs/GaAs [13] for dislocation management. Thick buffers requiring long growth time limit the process throughput. Furthermore, buffers made of III–V ternary alloys are particularly undesirable due to their poor thermal conductivity [14]. Recent advances in nanopatterned (NP) growth and epitaxial lateral overgrowth (ELOG) shed light on the heteroepitaxy of highly mismatched III–V semiconductors on Si substrates [15,16]. By modifying the lattice relaxation at the early stage of the heteroepitaxy [17,18] and trapping dislocations using the aspect ratio trapping technique [19–21], improved crystalline quality with reduced buffer thickness is possible. To date, heteroepitaxy of uncoalesced InP on Si substrates using patterned growth has been reported [15,16,19–21]. However, the growth of coalesced InP on nanostructured Si with high crystalline quality and smooth surface morphology suitable for device applications has not been fully explored.

In this paper, we report epitaxial growth of coalesced InP on NP-Si with position-controlled seed arrays using metal–organic chemical vapor deposition (MOCVD). By localizing defects inside the buried Si concaves during the initial seed layer deposition and promoting defect annihilation during the overgrowth process, a significant reduction in defect density with respect to the blanket growth was achieved. High resolution x-ray diffraction (HRXRD), scanning electron microscopy (SEM), and transmission electron microscopy (TEM) were used to study the morphology and crystalline quality of the InP films on NP-Si (001) substrates.

* Corresponding author. Tel.: +852 2358 7049; fax: +852 2358 1485.
E-mail address: eekmlau@ust.hk (K.M. Lau).

http://dx.doi.org/10.1016/j.jcrysgro.2014.07.052
0022-0248/© 2014 Elsevier B.V. All rights reserved.

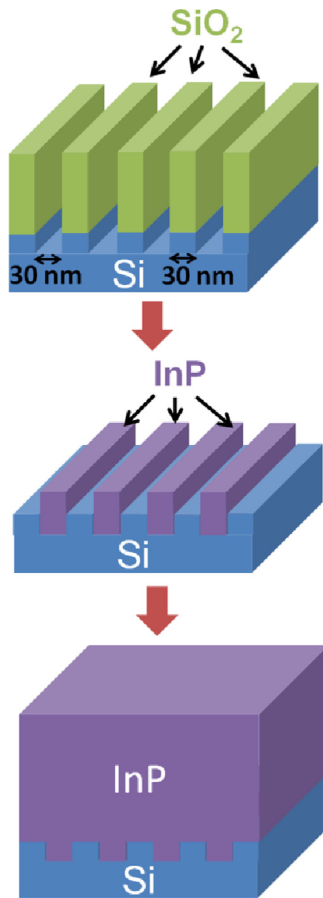

Fig. 1. Growth procedure of InP on nanostructured Si with a position-controlled seed array.

2. Experimental methods

Exact Si (001) substrates compatible with the mainstream Si manufacturing technology were used in the experiment. A 160 nm SiO_2 layer was first formed on the Si surface. Top-down lithography and dry etching were utilized to define [110] direction SiO_2 trench patterns. Si concaves 20 nm deep were formed inside the trenches. The trench width was 30 nm, with a SiO_2 spacing of 30 nm. The material growth was carried out in an Aixtron AIX-200/4 MOCVD system with a total gas flow rate of 15 slm. Prior to growth, the patterned Si was dipped in diluted HF solution briefly to remove native silicon oxide. Afterwards, the sample was heated up to 800 °C in the MOCVD chamber and annealed in pure H_2 ambient for 30 min for oxide desorption. AsH_3 was introduced at the end of the annealing process and the reactor was cooled down to the growth temperature. The growth of InP was performed using a modified two-step method, as illustrated in Fig. 1. Firstly, selective area growth (SAG) of InP seeds inside the 30 nm-wide trenches was carried out. To facilitate InP nucleation on the Si surface, the SAG was initiated with a ~5 nm GaAs wetting layer deposited at 400 °C. On top of the thin GaAs layer, we grew a few tens of nanometer thick InP seeds at temperatures of 450 °C and 550 °C. Then, the growth was stopped and the SiO_2 pattern was removed by buffered oxide etch, leaving a position-controlled nanoscopic InP seed array on the Si surface. On top of such InP seed array template, MOCVD overgrowth of coalesced InP proceeded at temperatures ranging from 600 °C to 650 °C.

The growth method presented in this work combines the concepts of conventional two-step method [10,11] and ELOG [16] but differs from them in the following aspects. In the conventional two-step growth technique, a low-temperature nucleation layer constructed by small and dense islands was deposited first at the kinetics-limited growth regime. The islands then coalesced to form a smooth, continuous but yet defective layer, which acted as the

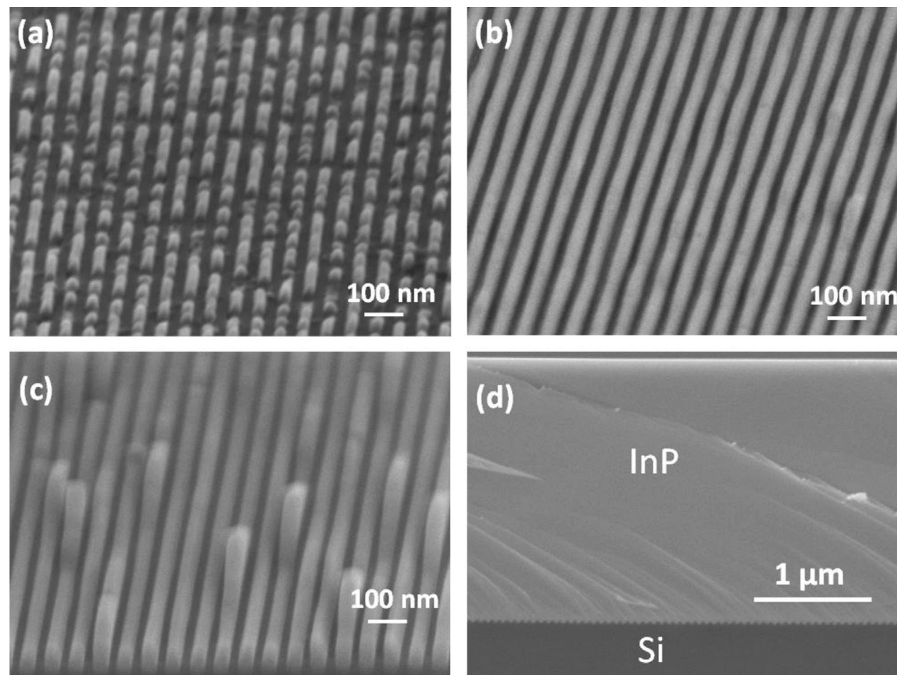

Fig. 2. 70° tilted SEM images of InP seed arrays with thicknesses of 30 nm (a), 50 nm (b), and 80 nm (c) and the cross-sectional SEM image of a 2.3 μm coalesced InP film overgrown on the seed array (d).

platform for the deposition of high quality overgrown layer in the second growth step at high temperature. This two-step scheme, however, is not applicable to the direct growth of InP on Si. Due to the large lattice mismatch between InP and Si as well as the long diffusion length of the Indium adatoms, InP tends to form large and sparse islands when directly grown on unpatterned planar Si substrates. In this work, the nucleation layer was restricted inside the trenches so that nano-sized position-controlled InP seeds can be realized. Moreover, the defects generated at the interface between Si and InP could be partially confined inside the Si concaves. The resultant small, dense, uniform and less defective InP seeds can serve as a better template for the subsequent overgrowth. The dielectric mask, however, can result in the formation of new stacking faults [16] or twin defects [22], as observed in traditional ELOG process. Therefore, we removed the SiO_2 sidewalls before the overgrowth to eliminate generation of new defects at the InP/SiO_2 interfaces.

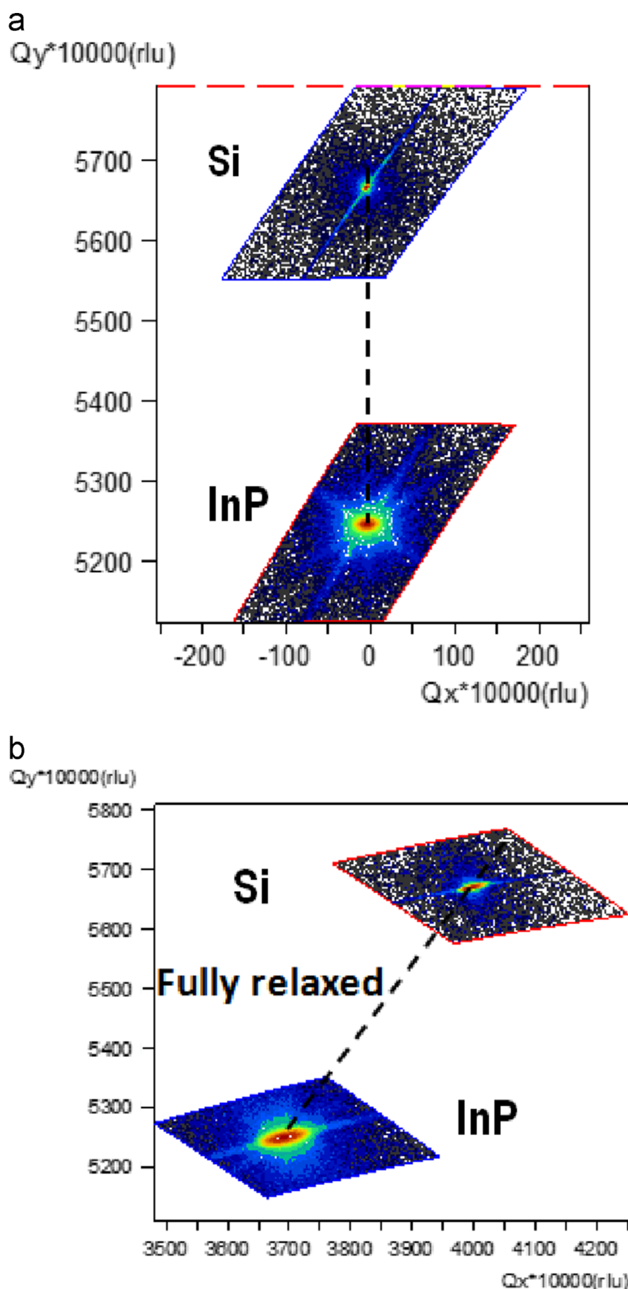

Fig. 3. (004) symmetric (a) and (224) asymmetric (b) reciprocal space mapping measured from a 2.3 μm-InP film.

3. Results and discussion

Prior to the overgrowth, we examined the morphology of the InP stripes (seed arrays) with SEM. Fig. 2(a)–(c) displays 70° tilted SEM images of the selectively deposited InP seed stripes with varied growth time. The SiO_2 mask had been removed before SEM observation and the corresponding InP seed layer thickness (t_{seed}) was approximately 30, 50 and 80 nm. According to Fig. 2(a), nano-sized InP islands nucleated in the trenches at the early stage of the heteroepitaxy. As growth proceeded, line-shaped seed array appeared (Fig. 2(b)). Further increasing the time for InP SAG led to increased fluctuation of t_{seed} (Fig. 2(c)). This could be related to varied adatom attachment rate resulting from the non-uniform distribution of strain states along the trenches [17]. Growth is more favored at sites with less stress, thus giving rise to the observed spatial variation in growth rates. The surface morphology of the seed layer turns out to have great impact on the crystalline quality of the subsequently overgrown InP film. This is to be discussed in more details shortly. Fig. 2(d) displays the cross-sectional SEM image of a 2.3 μm coalesced InP film overgrown on the seed array. The overgrown layer is smooth and the seeding stripes merge together seamlessly without any voids in between.

The crystalline quality and lattice relaxation of the coalesced InP was investigated using an Empyrean HRXRD system working at 40 kV voltage and 40 mA current with Cu Kα1 radiation. A hybrid monochromator consisting of an x-ray mirror and a two-crystal Ge (220) two-bounce monochromator was used to provide conditioned incident x-ray beam. A PIXcel detector was used for fast collection of the reciprocal space mapping (RSM). A channel-cut Ge analyzer crystal was employed to convert the diffractometer to triple axis mode for coupled $\omega/2\theta$ scans and ω-rocking curve scans. Fig. 3(a) presents the intensity contour plots of (004) symmetric RSM for a 2.3 μm coalesced InP film on NP-Si. The InP and Si peaks aligned vertically, whereas the elongated InP spot in the $k_{[110]}$ direction suggests mosaic spread. Fig. 3(b) plots (224) asymmetric RMS from the same sample. The diffracted intensity spot of InP fell on the diagonal line joining the (224) reciprocal lattice point of the Si substrate and the origin of the reciprocal space, indicating a fully relaxed InP layer. To evaluate the defect density quantitatively, x-ray $\omega/2\theta$ scans and ω-rocking curve scans of the (004) refection were performed. For nanopatterned growth, samples NP-1, NP-2, NP-3, NP-4 and NP-5 with various t_{seed} and overall InP thickness (t_{InP}) have been prepared. To facilitate comparison with blanket epitaxy, a 2.3 μm thick composite buffer composed of 1.3 μm-InP/1 μm-GaAs was grown on a planar Si substrate as a reference sample. The InP layer in the reference sample was grown by a two-step procedure [10,11]. A nucleation layer was first introduced at a relatively low-temperature (LT) of

Table 1
HRXRD FWHM values of ω-rocking curves and $\omega/2\theta$ curves measured from InP grown on nanopatterned (NP) Si and blanket Si (reference).

Sample	t_{seed} (nm)	t_{InP} (μm)	ω-FWHM$_\perp$ (arcsec)	ω-FWHM$_\parallel$ (arcsec)	$\omega/2\theta$-FWHM (arcsec)
NP-1	**30**	**1.3**	**518**	**687**	**105**
NP-2	**30**	**2.3**	**396**	**532**	**80**
NP-3	**50**	**2.3**	**360**	**565**	**78**
NP-4	**80**	**1.3**	**468**	**900**	**117**
NP-5	**80**	**2.3**	**410**	**709**	**92**
Reference	**1 μm GaAs + 110 nm LT-InP**	**1.3**	**766**	**911**	**116**

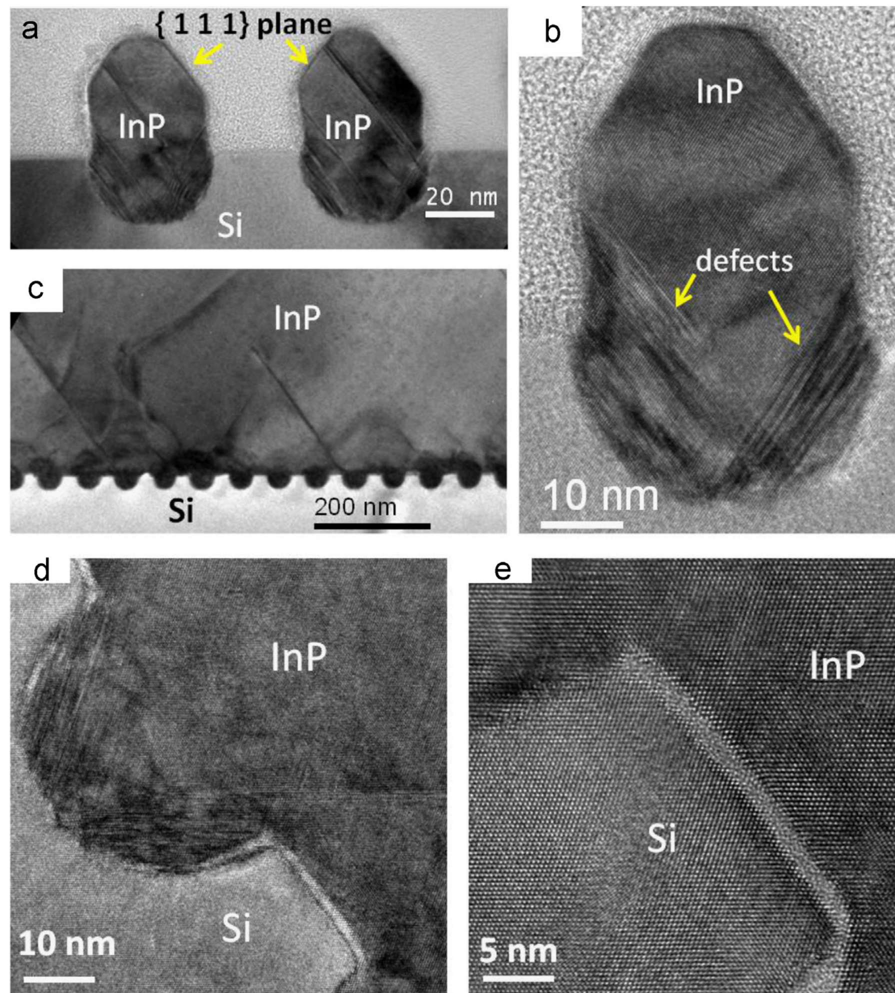

Fig. 4. (a) and (b) Cross-sectional TEM images of an InP seed array; (c) cross-sectional TEM image in the vicinity of the InP/Si interface after InP lateral overgrowth; (d) high resolution TEM image consisting of one concave and one Si ridge; (e) high resolution TEM image of the InP/Si interface on the Si ridge.

450 °C, followed by an InP overgrown layer deposited at a typical high temperature (HT) of 630 °C. AFM studies revealed that the LT-InP nuclei are mostly stripe-shaped, aligning along the [1$\bar{1}$0] direction, although no pre-defined pattern was used. As a consequence, during the HT-InP overgrowth, the probability for defect interactions could be slightly higher in the [110] direction relative to the [1$\bar{1}$0] direction. Table 1 compares the full-width-at-half-maximum (FWHM) values from InP on NP-Si and planar Si. Under the $\omega/2\theta$ scan modes, a 2.3 μm coalesced InP layer on NP-Si achieved a FWHM as narrow as 78 arcsec, 33% smaller than that of the reference sample (116 arcsec). Under the ω scan modes, a dependency of FWHM upon the incident x-ray direction was observed for all the samples. The FWHM value attained when the incident x-ray beam was aligned perpendicularly to the underlying InP seed stripes (ω-FWHM$_{\perp}$) is considerably smaller than the FWHM with x-ray aligned in parallel (ω-FWHM$_{\parallel}$). For the planar growth, the ω-FWHM$_{\perp}$ was defined as the FWHM value in the [110] direction, whereas the ω-FWHM$_{\parallel}$ was defined as the FWHM value in the [1$\bar{1}$0] direction. Compared to the reference sample, samples NP-2 and NP-3 achieved ~50% and ~40% reductions in ω-FWHM$_{\perp}$ and ω-FWHM$_{\parallel}$, respectively, with the same total buffer thickness of 2.3 μm. On the other hand, sample NP-1, with the same InP thickness as the reference, exhibited a ~30% reduction in both ω-FWHM$_{\perp}$ and ω-FWHM$_{\parallel}$. Using a thicker InP seed array in samples NP-4 and NP-5, we found a minimum change in ω-FWHM$_{\perp}$ but greatly broadened ω-FWHM$_{\parallel}$ compared with NP-1 and NP-3. It is possibly related to the large bumps observed in Fig. 2(c) and the poorer crystalline quality of thick InP seed layer deposited at low growth temperature. The best ω-scan FWHM of our heteroepitaxial InP layers on NP-Si outperforms other published FWHM values for ~2 μm thick InP on planar GaAs substrates [23,24], signifying effective defect trapping and reduction effect in nanopatterned growth. These results suggest that using nanostructured Si substrates, heteroepitaxy of InP with largely improved crystalline quality can be achieved without adding transitional buffers involving ternary alloys with poor thermal resistivity.

The defect trapping and reduction mechanism in the InP layer was investigated by TEM. We first looked at the defects in the Si concaves. Fig. 4(a) displays the cross-sectional TEM image of an InP seed array with the SiO_2 dielectric mask removed before the overgrowth. The growth fronts of the InP seed stripes exhibited {111} sidewalls and (001) top facets. A higher magnification TEM image of the cross-section is shown in Fig. 4(b). A large number of {111} plane defects were generated at the InP/Si interface. Some of these defects terminated at the sidewall of the Si concaves, whereas the rest of them glided to the perimeter of the seed layer outside the Si concaves and continued to propagate into the overgrown InP, as evidenced by the TEM image in Fig. 4(c). These observations suggest that deeper Si concaves with higher aspect ratio are desirable to trap all the defects generated inside the concaves. Next we studied the hetero-interface between InP and Si on the Si ridges outside the concaves. Fig. 4(d) shows a high resolution TEM image consisting of a concave and its neighboring

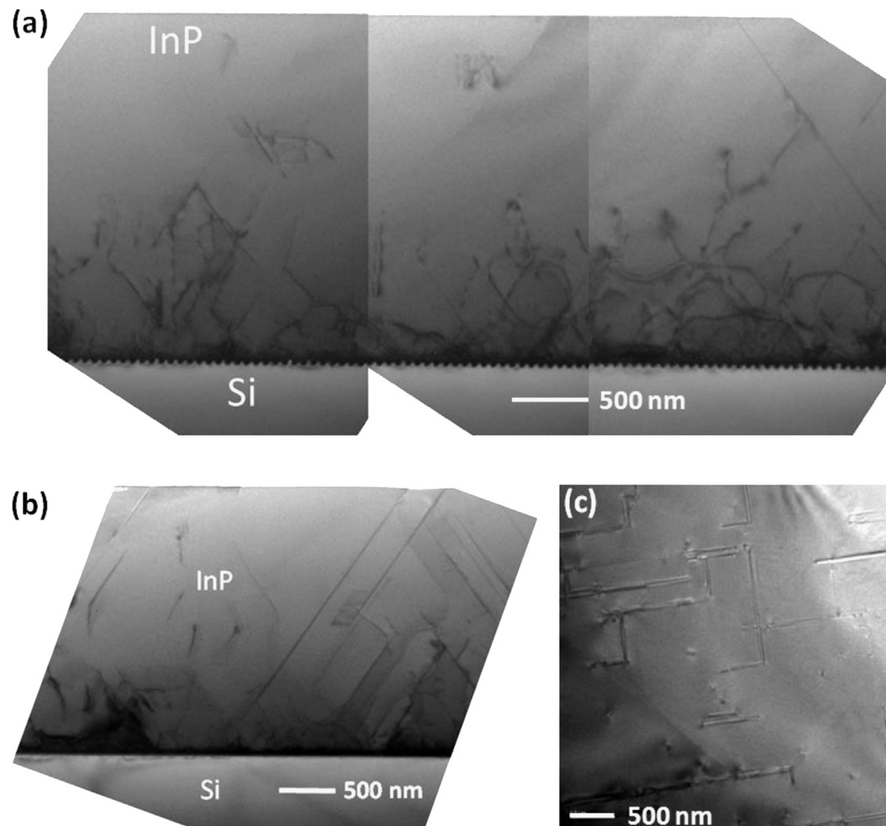

Fig. 5. TEM image of a coalesced InP film observed from the plane perpendicular to the seed stripes (a) and from the plane parallel to the seed stripes (b), and plan-view TEM image for InP-on-Si (c).

Si ridge. While a lot of stacking faults are found inside the concave, no new defects are generated at the Si ridge. This is further confirmed by the high magnification TEM image in Fig. 4(e). Interestingly, we observed an ultra-thin amorphous layer with thickness of less than 1 nm between Si and InP. The amorphous layer is possibly the native silicon oxide formed before the overgrowth. Compared to the high density defects inside the concaves, almost no threading defects were introduced on the Si ridges. This is probably because the InP seeds from adjacent concaves grew laterally on the Si ridge and had reached full relaxation by the time they merged together. These observations indicate that the defect density in the coalesced InP can be further decreased by increasing the distance between the Si concaves.

Fig. 5(a) presents the cross-sectional TEM image of a 2.3 μm coalesced InP film observed from the plane perpendicular to the seed stripe direction. Clearly, bending and annihilation of the dislocations occurred during the overgrowth and coalescence processes. Most of the defects vanished after they intersected with each other, leading to a significantly reduced defect density in the upper 1 μm InP layer. Fig. 5(b) shows the TEM image observed from the plane parallel to the seed stripe direction. Compared with the perpendicular view, higher-density {111} plane defects (stacking faults/twins) propagating to the InP surface were observed. The measured higher defect density along the SiO_2 trench direction is reasonable because there is no defect trapping effect during the seed layer deposition and reduced likelihood for dislocation interactions during the InP coalescence. Growth in this direction is more similar to the planar growth scenario. These findings are consistent with the abovementioned anisotropic FWHM values of the ω-rocking curves. Fig. 5(c) displays a plan-view TEM image. The defects were dominated by stacking faults and a defect density of $\sim 2\times10^8/cm^2$ was obtained. The defect density could be further reduced by thermal annealing or insertion of superlattices in the InP.

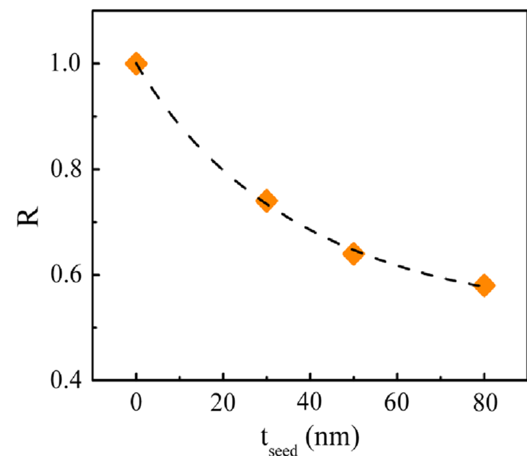

Fig. 6. ω-$FWHM_{\perp}$ to ω-$FWHM_{\parallel}$ ratio (R) of the coalesced InP films as a function of the underlying InP seed layer thickness.

The anisotropic defect distribution in the coalesced InP films on NP-Si was found to be dependent on the underlying seed layer thickness. The ω-$FWHM_{\perp}$ to ω-$FWHM_{\parallel}$ ratio (R) was plotted as a function of t_{seed} in Fig. 6. For the ideal two-dimensional growth with isotropic FWHM, $R=1$. In terms of nanopatterned growth, the thinner the seed layer, the higher the R (closer to 1). It can be explained by the fact that the initial seed array pattern can deform the subsequent overgrowth process. An island-shaped thin InP seed array is more effective in distributing mismatched strain in three dimensions [18]. As a result, the dislocations climbed to the island perimeter and then interacted with each other efficiently in

the following overgrowth process. On the contrary, thicker stripe-like InP seed arrays promote the anisotropic strain relaxation and defect interactions along the [110] and [1$\bar{1}$0] directions.

4. Conclusions

In conclusion, we reported MOCVD growth of InP on nanopatterned exact Si (001) substrates with position-controlled seed arrays. The defects were partially trapped in the buried Si concaves and partially reduced during the following overgrowth process. Significantly reduced x-ray linewidth has been achieved with respect to the planar growth approach. TEM studies revealed the anisotropic distribution of defects, which stemmed from the anisotropic strain relaxation and defect interactions along [110] and [1$\bar{1}$0] directions. The approach in this study can be applied to the mismatched growth of a large variety of III–V semiconductors on Si substrates, potentially facilitating the monolithic integration of Si technologies with III–V functionalities.

Acknowledgments

This work was supported in part by Grants (614312 and 614813) from the Research Grants Council of Hong Kong. The authors would like to thank Thomas Kuech, Jun Ma, Chao Liu and Yu Geng for many helpful discussions and the MCPF of HKUST for the technical support.

References

[1] Y. Bai, S. Slivken, S. Kuboya, S.R. Darvish, M. Razeghi, Quantum cascade lasers that emit more light than heat, Nat. Photonics 4 (2010) 99.
[2] L. Xu, M. Nikoufard, X.J.M. Leijtens, T.D. Vries, E. Smalbrugge, R. Nötzel, Y.S. Oei, M.K. Smit, High-performance InP-based photodetector in an amplifier layer stack on semi-insulating substrate, IEEE Photonics Technol. Lett. 20 (2008) 1941.
[3] R. Lövblom, R. Flückiger, M. Alexandrova, O. Ostinelli, C.R. Bolognesi, InP/GaAsSb DHBTs with simultaneous $f_T/f_{MAX}=428/621$ GHz, IEEE Electron Device Lett. 34 (8) (2013) 984.
[4] D.-H. Kim, B. Brar and J.A. del Alamo, $f_T=688$ GHz and $f_{max}=800$ GHz in $L_g=40$ nm $In_{0.7}Ga_{0.3}As$ mHEMTs with $g_{m,max}>2.7$ mS/μm, in: Proceedings of the IEEE International Electron Devices Meeting, 2011, 319.
[5] J.A. del Alamo, Nanometer-scale electronics with III–V compound semiconductors, Nature 479 (7373) (2011) 317.
[6] R. Chau, B. Doyle, S. Datta, J. Kavalieros, K. Zhang, Integrated nanoelectronics for the future, Nat. Mater. 6 (2007) 810.
[7] H. Kataria, C. Junesand, Z. Wang, W. Metaferia, Y.T. Sun, S. Lourdudoss, et al., Towards a monolithically integrated III–V laser on silicon: optimization of multi-quantum well growth on InP on Si, Semicond. Sci. Technol. 28 (2013) 094008.
[8] Y. Kohama, Y. Kadota, Y. Ohmachi, InP grown on Si substrates with GaP buffer layers by metal–organic chemical vapor deposition, Jpn. J. Appl. Phys. 28 (1989) 1337.
[9] O. Aina, M. Mattingly, J.R. Bates, A. Coggins, J. O'Connor, S.K. Shastry, et al., High-purity InP grown on Si by organometallic vapor phase epitaxy, Appl. Phys. Lett. 58 (1991) 1554.
[10] Q. Li, C.W. Tang, K.M. Lau, Growth of ultra-high mobility $In_{0.52}Al_{0.48}As$/$In_xGa_{1-x}As$ ($x \geq 53\%$) quantum wells on Si substrates using InP/GaAs buffers by metal–organic chemical vapor deposition, Appl. Phys. Express 7 (2014) 045502.
[11] Q. Li, X. Zhou, C.W. Tang, K.M. Lau, Material and device characteristics of metamorphic $In_{0.53}Ga_{0.47}As$ MOSHEMTs grown on GaAs and Si substrates by MOCVD, IEEE Trans. Electron Devices 60 (2013) 4112.
[12] W.K. Liu, D. Lubyshev, J.M. Fastenau, Y. Wu, M.T. Bulsara, E.A. Fitzgerald, et al., Monolithic integration of InP-based transistors on Si substrates using MBE, J. Cryst. Growth 311 (2009) 1979.
[13] N. Mukherjee, J. Boardman, B. Chu-Kung, G. Dewey, A. Eisenbach, J. Fastenau et al., MOVPE III–V material growth on silicon substrates and its comparison to MBE for future high performance and low power logic applications, in: Proceedings of the IEEE International Electron Devices Meeting, 2011, 821.
[14] W. Nakwaski, Thermal conductivity of binary, ternary, and quaternary III–V compounds, J. Appl. Phys. 64 (1988) 159.
[15] J.G. Fiorenz, J.-S. Park, J.M. Hydrick, J. Li, J.Z. Li, M. Curtinb, M. Carroll, A. Lochtefeld, Aspect ratio trapping: a unique technology for integrating Ge and III–Vs with silicon CMOS, ECS Trans. 33 (2010) 963.
[16] C. Junesand, H. Kataria, W. Metaferia, N. Julian, Z. Wang, Y. Sun, et al., Study of planar defect filtering in InP grown on Si by epitaxial lateral overgrowth, Opt. Mater. Express 3 (2013) 1960.
[17] T.F. Kuech, L.J. Mawst, Nanofabrication of III–V semiconductors employing diblock copolymer lithography, J. Phys. D: Appl. Phys. 43 (2010) 183001.
[18] A. Bakin, D. Piester, I. Behrens, H.-H. Wehmann, E. Peiner, A. Ivanov, et al., Growth of InP layers on nanometer-scale patterned Si substrates, Cryst. Growth Des. 3 (2003) 89.
[19] J.Z. Li, J. Bai, J.M. Hydrick, J.G. Fiorenza, C. Major, M. Carroll, et al., Thin film InP epitaxy on Si (001) using selective aspect ratio trapping, ECS Trans. 18 (2009) 887.
[20] C. Merckling, N. Waldron, S. Jiang, W. Guo, O. Richard, B. Douhard, et al., Selective area growth of InP in shallow trench isolation on large scale Si (001) wafer using defect confinement technique, J. Appl. Phys. 114 (2013) 033708.
[21] M. Paladugu, C. Merckling, R. Loo, O. Richard, H. Bender, J. Dekoster, et al., Site selective integration of III–V materials on Si for nanoscale logic and photonic devices, Cryst. Growth Des. 12 (2012) 4696.
[22] S. Jha, C.-C. Liu, T.S. Kuan, S.E. Babcock, P.F. Nealey, J.H. Park, et al., Defect reduction in epitaxial GaSb grown on nanopatterned GaAs substrates using full wafer block copolymer lithography, Appl. Phys. Lett. 95 (2009) 062104.
[23] M.B. Derbali, J. Meddeb, H. Mâaref, D. Buttard, P. Abraham, Y. Monteil, A comparative study of heterostructures InP/GaAs (001) and InP/GaAs (111) grown by metal–organic chemical vapor deposition, J. Appl. Phys. 84 (1998) 503.
[24] P.A. Postigo, F. Suárez, A. Sanz-Hervás, J. Sangrador, C.G. Fonstad, Growth of InP on GaAs (001) by hydrogen-assisted low-temperature solid-source molecular beam epitaxy, J. Appl. Phys. 103 (2008) 013508.